PHYSICAL REVIEW D

PARTICLES AND FIELDS

THIRD SERIES, VOLUME 25, NUMBER 9 1 MAY 1982

Study of $\bar{p}p$ annihilation into channels with one or more K_S^0 in the incident-momentum range 403 to 670 MeV/c

Y. Kubota,* F. Sai, S. Sakamoto, F. Shimizu, and S. S. Yamamoto
Department of Physics, University of Tokyo, Bunkyo-ku, Tokyo 113, Japan
(Received 14 January 1982)

We measured exclusive cross sections for $\bar{p}p$ annihilation into channels with one or more K_S^0 at six incident momenta from 403 to 670 MeV/c. No energy dependence was observed in these cross sections, nor was there any energy dependence in the fractions of various resonances produced in three- and more-body annihilation channels. Taken together with the data of Petitjean, there seems to be a weak indication of a broad enhancement in the $\bar{p}p \to K_S^0 K_L^0$ cross section at an incident momentum of around 500 MeV/c. The angular distribution of K_S^0 suggests the presence of the $^3D_1$ and/or $^3D_3$ partial-wave amplitude in this channel.

I. INTRODUCTION

As part of our continuing effort to study all aspects of antiproton-proton interactions in the incident-momentum range 370 to 730 MeV/c, which covers the now somewhat controversial $S(1936)$ meson, we undertook to study antiproton-proton annihilation into channels with at least one visible K_S^0. Data on these channels exist for annihilation at rest[1,2] and 700[3,4] and 1200 MeV/c,[5,6] but hardly any data exist in our momentum range. The only data that do exist are on the $\bar{p}p \to K_S^0 K_L^0$ channel,[7-9] of which one set of data[7] is in disagreement with the others, and on the $\bar{p}p \to K_S^0 K^{\pm}\pi^{\mp}$ channel.[10] Therefore, the purpose of this study was to fill the gap in the data on these annihilation channels with at least one visible K_S^0, and to compare our data with those at rest and at the higher momenta to see if there was any momentum-dependent behavior in cross sections both for the observed final states and for resonance production in some of the final states. (The data at rest and at the higher momenta show copious production of resonances in many three- and more-body final states.)

II. EXPERIMENTAL PROCEDURES

This study is based on 245 000 pictures obtained from the Columbia-BNL 30-in. liquid hydrogen bubble chamber at the Brookhaven Alternating Gradient Synchrotron (AGS) exposed to a low-energy separated beam of antiprotons, whose nominal momenta at the center of the bubble chamber were 403, 480, 537, 584, 630, 670, 697, and 728 MeV/c. In this study, about 205 000 pictures taken at the lower six momenta were used. The details of the experimental setup are given in Ref. 11.

The contamination of the beam by π^-'s and μ^-'s was estimated to be 10%. These tracks could be identified unambiguously from their bubble densities, and were duly taken care of in the flux counting for the total-cross-section measurement.[11]

Even though the amount of contamination was expected to be much smaller than that by π^-'s and μ^-'s, a potentially more troublesome contamination was by K^-'s, since K^-'s would produce $\bar{K}^0$ and Λ at our beam momenta, which could simulate the reactions of interest. The bubble density of K^- tracks was such that they were not easily identifiable. We, therefore, estimated the contamination of the beam by the K^- from the number of Λ's produced by the beam tracks, and for the 670-MeV/c exposure, from the number of τ decays in the beam tracks as well. A total of four Λ's found this way and one τ decay correspond to a contamination of 0.08%. (We used an average cross section of 5 mb for Λ production by K^- in our momentum range to arrive at this figure.)

TABLE I. Number of events for each topology at each incident momentum.

Topology	Momentum (MeV/c) 403	480	537	584	630	670	Total
0P1V	75	45	53	37	53	46	309
0P2V	12	9	17	8	18	13	77
2P1V	342	285	298	238	308	244	1715
2P2V	54	36	59	30	34	33	246
4P1V	12	12	8	9	16	10	67
All	495	387	434	322	429	346	2414

The entire film was double scanned for event topologies involving at least one vee. Each topology was designated as nPmV, where n is the number of the secondary charged particles at the production vertex and m is that of the vees. The topologies of interest were: 0P1V, 0P2V, 2P1V, 2P2V, and 4P1V.

A total of about 2400 events was found. The number of events for each topology of interest at each momentum is listed in Table I. The scanning efficiencies for the topologies involved are listed in Table II. All events were measured and spatially reconstructed in a standard way.

In order to use only well measured events for further analyses, a fiducial volume was defined for the production vertex and another for the decay vertex. Events falling outside the fiducial volumes were rejected. The fiducial volume for the production vertex was 48 cm in diameter and 19 cm in depth, and that for the decay vertex was 52 cm in diameter and 27 cm in depth, both centered at the center of the bubble chamber.

The events which failed in the spatial reconstruction procedure were remeasured at most twice. The events which failed spatial reconstruction after the third measurement amounted to 1.2% of the total number of events, and were discarded. The cross sections were properly corrected for these events. Each spatially reconstructed event was fitted to various kinematical hypotheses depending on its topology. The kinematical hypotheses tried are listed below for each topology:

0P1V: $\bar{p}p \rightarrow K_S^0(K^0)$,

0P2V: $\bar{p}p \rightarrow K_S^0 K_S^0$,

$\bar{p}p \rightarrow K_S^0 K_S^0 \pi^0$,

2P1V: $\bar{p}p \rightarrow K_S^0 K^{\pm}\pi^{\mp}$,

$\bar{p}p \rightarrow K_S^0 K^{\pm}\pi^{\mp}\pi^0$,

$\bar{p}p \rightarrow K_S^0(K^0)\pi^+\pi^-$,

2P2V: $\bar{p}p \rightarrow K_S^0 K_S^0 \pi^+\pi^-$,

$\bar{p}p \rightarrow K_S^0 K_S^0 \pi^+\pi^-\pi^0$,

4P1V: $\bar{p}p \rightarrow K_S^0 K^{\pm}\pi^{\mp}\pi^+\pi^-$,

$\bar{p}p \rightarrow K_S^0 K^{\pm}\pi^{\mp}\pi^+\pi^-\pi^0$,

$\bar{p}p \rightarrow K_S^0(K^0)2\pi^+2\pi^-$,

TABLE II. Scanning efficiency (in %) for each topology at each incident momentum.

Topology	Momentum (MeV/c) 403	480	537	584	630	670	Average
0P1V	94	96	97	98	94	93	96
0P2V	89	96	100	100	98	100	100
2P1V	96	98	98	98	96	96	97
2P2V	98	100	100	100	100	100	100
4P1V	89	93	98	92	85	89	90
Average	96	98	98	99	96	97	98

where (K^0) means missing K^0 or $\bar{K}^0$.

III. EVENT IDENTIFICATION

A. K_S^0 identification

In the above kinematical fitting, vee's were always fitted to the hypothesis $K_S^0 \to \pi^+\pi^-$ first with its direction as known [three-constraint (3C) fit], and if this failed, with its direction as unknown (1C fit). Since in our momentum range $\bar{p}$'s do not produce the Λ, all vee's were fitted to this hypothesis only. A vee whose fitting probability to the 3C K_S^0 decay hypothesis was greater than 0.1% was accepted as a K_S^0. A vee which did not meet this 3C criterion, but fitted the 1C K_S^0 decay hypothesis with a fitting probability of 0.1% was also accepted as a K_S^0, if the difference between its direction obtained from the fit and its measured direction was within the error of the measurement. The kinematical fitting program does not always work properly when some of the input values have large errors. There were many vee's with short decay lengths with large errors in their directions, and the above identification procedure was used to avoid inlcuding spurious K_S^0 events.

Furthermore, we chose a minimum decay length in order to correct properly for the loss due to K_S^0's which decayed too close to the production vertex. The decay length of each K_S^0 was projected on the fiducial plane (the inside surface of the bubble-chamber window) as seen in the scanned view. The cutoff length was defined in terms of this projected decay length and was chosen to be 1.5 mm. The maximum decay length was either 12 cm or the potential length, whichever was shorter. Only those K_S^0's whose decay lengths fell within these limits were accepted.

In order to make certain that the above selection procedure was appropriate, the mass and the lifetime of the K_S^0 were obtained. The distribution of the $\pi^+\pi^-$ invariant mass of the vees which fitted the K_S^0 decay was fitted to a Breit-Wigner form. The resultant mass and mass resolution were $m = 497.2 \pm 0.3$ MeV/c^2 and $\Gamma = 9.8 \pm 0.3$ MeV/c^2. The lifetime was obtained using the maximum-likelihood method. The measured lifetime multiplied by the light velocity was 2.68 ± 0.17 cm. These values indicate that the selection procedure did not introduce any systematic effect.

B. Reaction identification

An event was accepted as fitting a particular reaction hypothesis if the fitting probability was

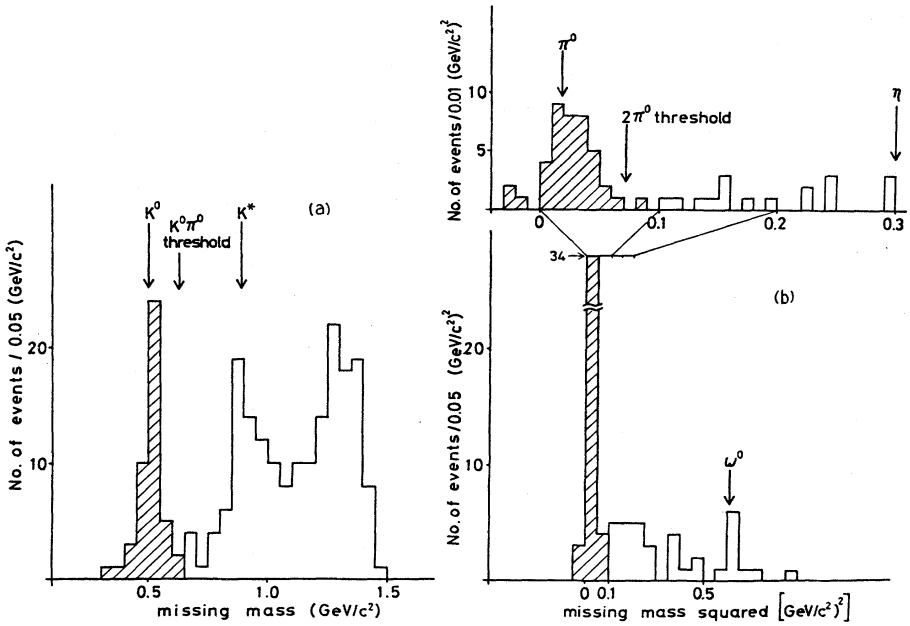

FIG. 1. (a) Missing-mass spectrum of 0P1V events. The shaded area corresponds to the events which fit the $K_S^0(K^0)$ hypothesis. (b) Missing-mass-squared spectrum of 0P2V events. The shaded area corresponds to the events which fit the $K_S^0 K_S^0 \pi^0$ hypothesis. The spectrum around the π^0 mass squared is expanded for clarity and is shown at the top of the figure.

greater than 0.1% and the bubble densities of the secondary particles (when applicable) were consistent with the hypothesis.

The missing-mass-squared (against K_S^0) spectra of 0P1V and 0P2V events are shown in Figs. 1(a) and 1(b). The shaded areas in Figs. 1(a) and 1(b) correspond to the events accepted as $K_S^0(K^0)$ and $K_S^0K_S^0\pi^0$ events, respectively. There is no narrow peak around zero missing mass squared in Fig. 1(b). The mass-squared region around the π^0 mass squared is enlarged for clarity and is shown in the top half of Fig. 1(b). Coupled with the fact that there was no acceptable fit to the $K_S^0K_S^0$ hypothesis, the absence of a peak at zero missing mass squared indicates the absence of $K_S^0K_S^0$ events.

The missing-mass-squared spectrum of 2P1V events with an identified K^+ or K^- as one of the charged prongs is shown in Fig. 2. The shaded areas correspond to the events fitting the $K_S^0K^{\pm}\pi^{\mp}$ hypothesis, the blank areas correspond to the events fitting the $K_S^0K^{\pm}\pi^{\mp}\pi^0$ hypothesis, and the filled areas are those events which did not fit any hypothesis successfully. In contrast to the previous case there is a clear narrow peak at zero missing mass squared, which corresponds to the $K_S^0K^{\pm}\pi^{\mp}$ events. A broader peak around the π^0 mass squared corresponds to the $K_S^0K^{\pm}\pi^{\mp}\pi^0$ events.

From these distributions we conclude that the identification of various reactions by kinematical fitting and ionization is quite unambiguous. There were, however, 40 events which remained ambiguous between two 1C hypotheses even after the bubble-density inspection. In the cross-section calculation these events were equally apportioned into the fitted reactions.

IV. CROSS-SECTION MEASUREMENT

A. Topological cross section

The cross section for a given topology σ_{top} at each incident momentum was calculated by the

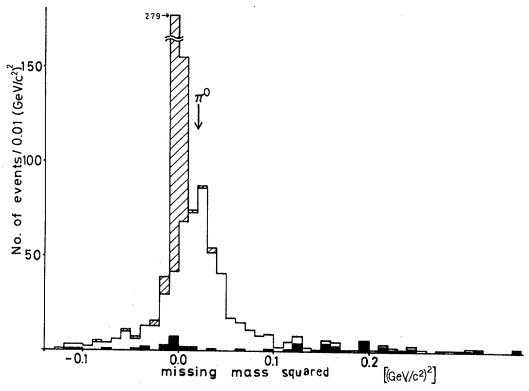

FIG. 2. Missing-mass-squared spectrum of $K_S^0K^{\pm}\pi^{\mp}+\text{MM}$ events. The shaded areas correspond to the events which fit the $K_S^0K^{\pm}\pi$ hypothesis, the blank areas to the events which fit the $K_S^0K^{\pm}\pi^{\mp}\pi^0$ hypothesis, and the filled areas to the events which did not fit any hypothesis.

formula

$$\sigma_{\text{top}}=\frac{\sigma_{\text{tot}}}{1-\exp(-l\rho N_0\sigma_{\text{tot}})}\frac{N_{\text{top}}}{N_f},$$

where σ_{tot}, l, and N_f are the total cross section, average beam path length, and the total beam flux obtained by Sakamoto *et al.*,[11] and N_{top}, N_0, and ρ are the number of events belonging to this topology, Avogadro's number, and the density of liquid hydrogen, 0.063 g/cm^3.

The topological cross sections are given in Table III for each momentum. They are corrected for the decay length limits. The same correction as well as the correction for the undetected decay modes were made (using the branching ratio $B=K_S^0\to\pi^+\pi^-/K_S^0\to\text{all}=0.686$) for the channel cross sections to be described in the next section.

The 0.08% contamination of the beam by K^- mentioned earlier would produce a total of about

TABLE III. Topological cross sections (in μb) at each incident momentum.

	Momentum (MeV/c)						
Topology	403	480	537	584	630	670	Average
0P1V	257±30	201±31	174±24	157±26	184±26	172±25	177±12
0P2V	44±13	44±15	60±15	40±14	68±16	51±14	54±7
2P1V	1168±65	1266±75	1002±59	1003±65	1056±60	897±58	1039±28
2P2V	198±29	175±31	221±29	132±25	127±22	127±22	157±12
4P1V	8±6	32±12	26±10	28±12	47±14	36±12	34±5
Total	1675±79	1718±89	1483±72	1360±77	1482±72	1283±69	1461±34

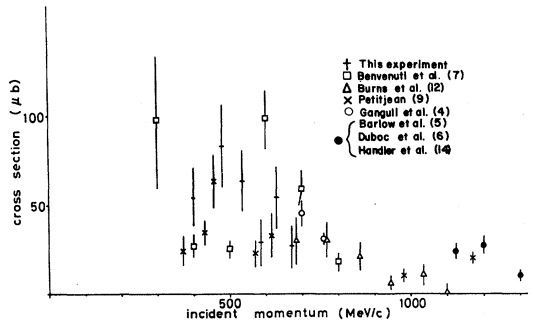

FIG. 3. $K_S^0K_L^0$ cross section versus incident momentum.

four 0P1V K_S^0 events, but no correction was made for these events. (We used 5 mb for the cross section for $K^-p \rightarrow \bar{K}^0n$ in our momentum range.)

B. Channel cross sections

Using the same cross-section formula as that used for the topological cross sections, various channel cross sections were calculated. These cross sections (except for those for the six-body final state) are plotted as functions of incident momentum in Figs. 3 and 4 together with the cross sections obtained by others.[3–7,9,12,13] The six-body cross sections are all essentially negligibly small.

V. TWO-BODY ANNIHILATION

The only two-body annihilation channel observed in this experiment is the $K_S^0K_L^0$ channel. As seen from Fig. 3 our cross sections fit in well with those obtained by Petitjean[9] and connect more or less smoothly to the data at higher momenta.[12] The cross sections obtained by Benvenuti *et al.*,[7] how-

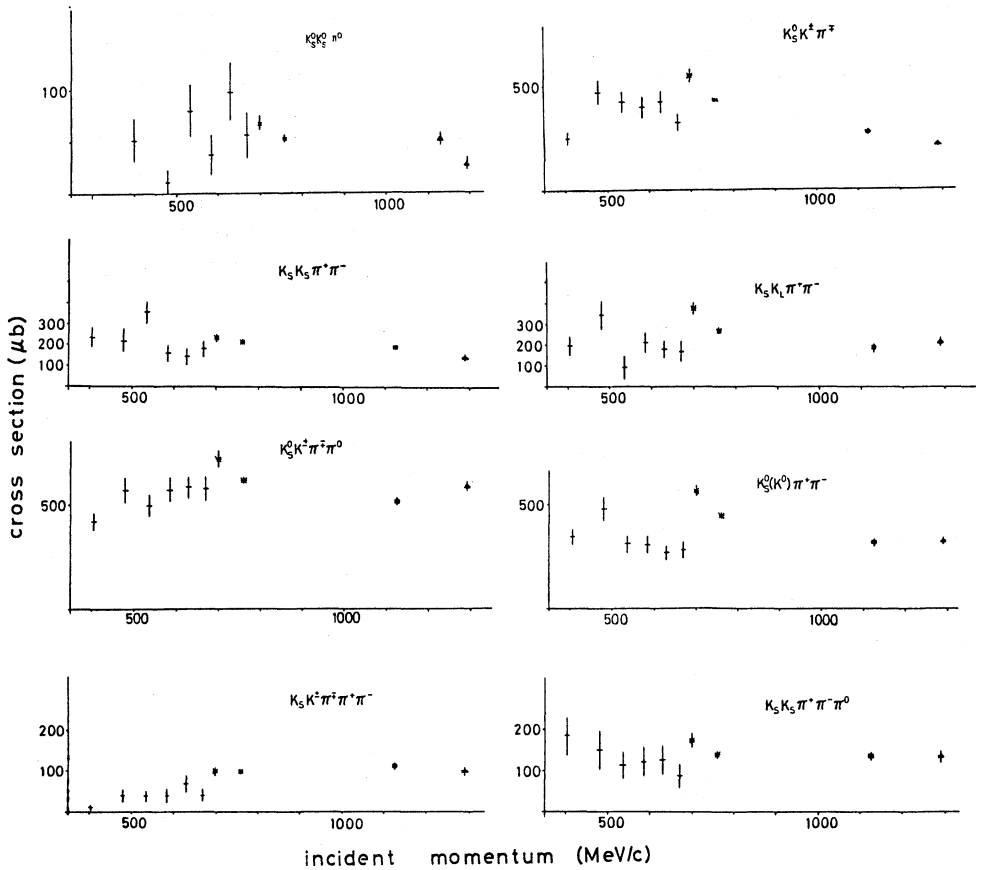

FIG. 4. Cross sections for three-, four-, and five-body final states with at least one K_S^0 versus incident momentum. The final states are indicated in the figures. The meanings of the symbols are as follows: +, this experiment; ×, Ganguli *et al.* (Ref. 4); ■, Duboc *et al.* (Ref. 6); and △, Handler *et al.* (Ref. 13), except for the $K_S^0K_S^0\pi^0$ state for which this represents data by Barlow *et al.* (Ref. 5) and Duboc *et al.* (Ref. 6).

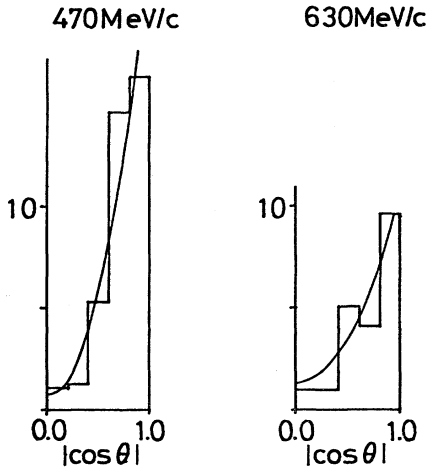

FIG. 5. Folded angular distributions of K_S^0 from the $K_S^0K_L^0$ events at 470 and 630 MeV/c.

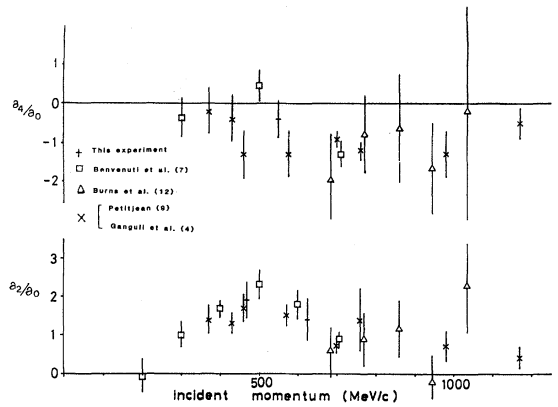

FIG. 6. Legendre-expansion coefficients a_2/a_0 and a_4/a_0 of the K_S^0 angular distribution from the $K_S^0K_L^0$ events versus incident momentum.

ever, disagree strongly with ours as well as Petitjean's.[9] If we only look at the cross sections obtained by Petitjean[9] and by us, there seems to be a weak indication of a broad enhancement around an incident momentum of 500 MeV/c. But the claim by Benvenuti *et al.*[7] that there is a narrow $J^P=1^-$ resonance at around 600 MeV/c is not supported by our data or by Petitjean's.[9]

The K_S^0 angular distribution was analyzed in terms of the Legendre expansion coefficients. Because of the paucity of the $K_S^0K_L^0$ events, the events were lumped into two momentum regions: 400–530 MeV/c and 580–670 MeV/c. The folded distributions at these momenta are shown in Fig. 5 where the solid curves represent the results of the Legendre polynomial expansion using the moment method. The coefficients obtained are shown in Fig. 6 together with the data from other experiments.[3,4,7,9] Unlike the result of Petitjean,[9] we found a_6/a_0 to be negligible.

All values of a_2/a_0 including those obtained by Petitjean[9] in our momentum range are large enough to be significant, suggesting a large contribution of the initial states $^{2S+1}L_J={}^3D_3$ and/or ${}^3D_1$; a pure D-wave initial state will give $a_2/a_0=1$, and a pure S wave, $a_2/a_0=0$. Therefore, the small cross-section enhancement at 500 MeV/c would correspond to a resonance with $J^P=1^-$ or 3^-, if taken seriously. However, this enhancement is not likely to be associated with the S meson, because its mass and width are larger than those of the S. If anything, it may be an excited state of ϕ, because of its decay into the $K_S^0K_L^0$ state.

VI. THREE-, FOUR-, AND FIVE-BODY ANNIHILATION

No momentum dependence is seen in the cross sections for these many-body annihilation channels as seen from Fig. 4. Our cross sections seem to connect to those at 1.13 (Refs. 5 and 6) and 1.3 GeV/c,[13] but not to those obtained at 0.7 GeV/c by Ganguli *et al.*,[4] which are higher than ours. This may indicate some systematic difference between our data and those by Ganguli *et al.*[4]

In order to investigate resonance production in

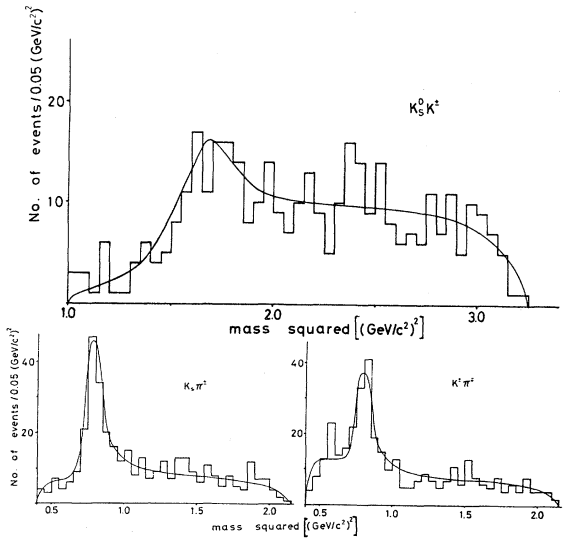

FIG. 7. The two-body effective-mass-squared distributions of the $K_S^0K^\pm\pi^\mp$ events. The mass combinations are indicated in the figures. See the text for the explanation of the solid curves.

the final states, two- and three-body effective-mass-squared distributions were obtained for various mass combinations from the final states $K_S^0K^{\pm}\pi^{\mp}$, $K_S^0K^{\pm}\pi^{\mp}\pi^0$, and $K_S^0\pi^+\pi^-(K^0)$. Only these final states had enough events to make the following analysis meaningful. Fig. 7 shows the two-body effective-mass-squared distributions from the $K_S^0K^{\pm}\pi^{\mp}$ final state. Figure 8 shows the two- and three-body effective-mass-squared distributions from the $K_S^0K^{\pm}\pi^{\mp}\pi^0$ final state. Figure 9 shows the two- and three-body effective-mass-squared distributions from the $K_S^0\pi^+\pi^-(K^0)$ final state. In many of these distributions production of resonances such as K^* and ϕ is clearly seen.

In order to obtain the fractions of resonance production in any given final state, we fitted all the effective-mass-squared distributions of a given final state to incoherent superpositions of the

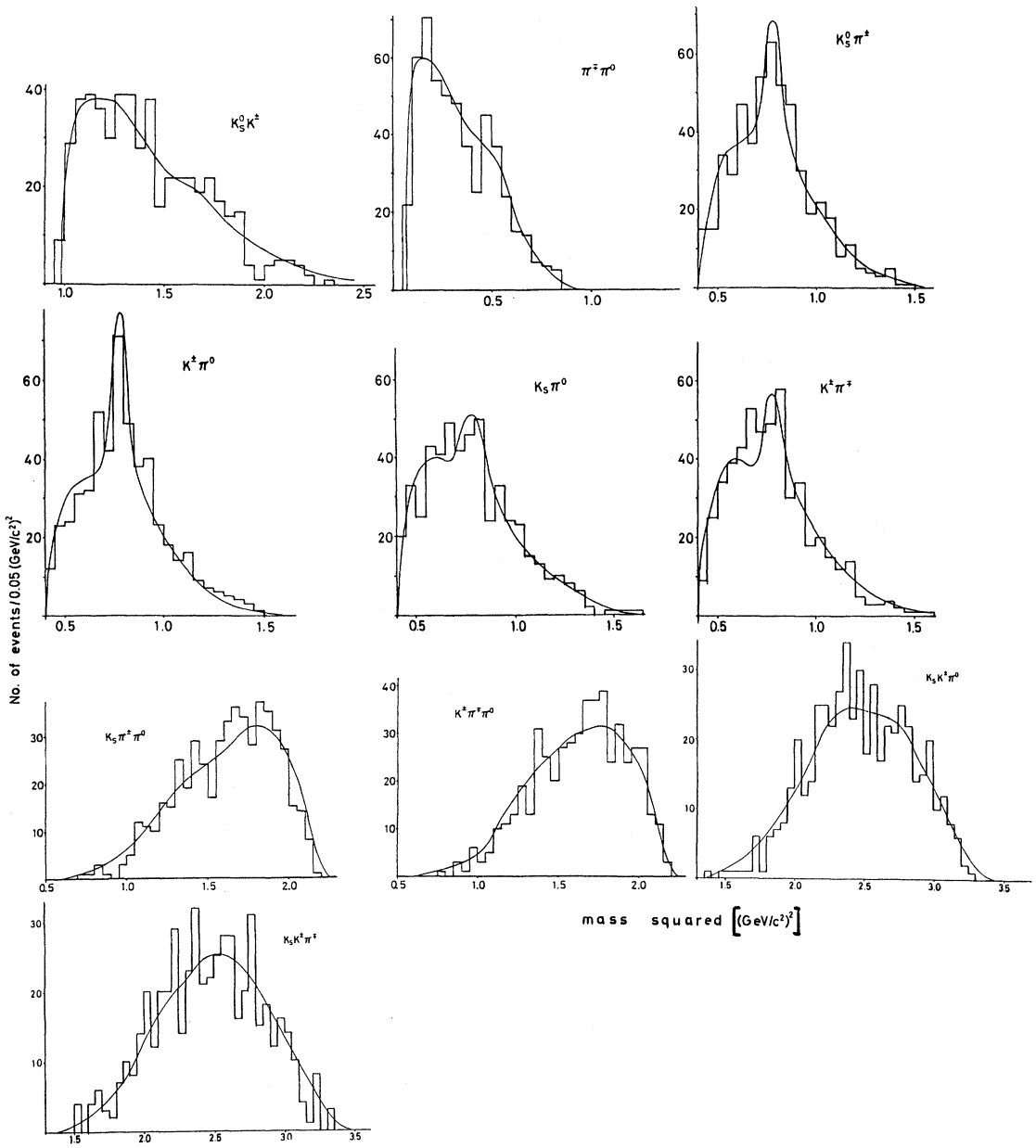

FIG. 8. The two- and three-body effective-mass-squared distributions of the $K_S^0K^{\pm}\pi^{\mp}\pi^0$ events. The mass combinations are indicated in the figures. See the text for the explanation of the solid curves.

effective-mass-squared distributions expected from intermediate states involving at least one resonance such as $K^*K\pi$, and phase space which included the effect of the threshold enhancement seen in the $K^{\pm}\pi^{\mp}$ mass-squared distribution (Fig. 7). This effect is denoted by $(K\pi)_{SL}$ and is represented by the zero-range scattering-length approximation $1/[1+(aq)^2]$, where q is the momentum of K in the $K\pi$ center-of-mass system, and a is a parameter to be fitted. The resonances considered were δ,

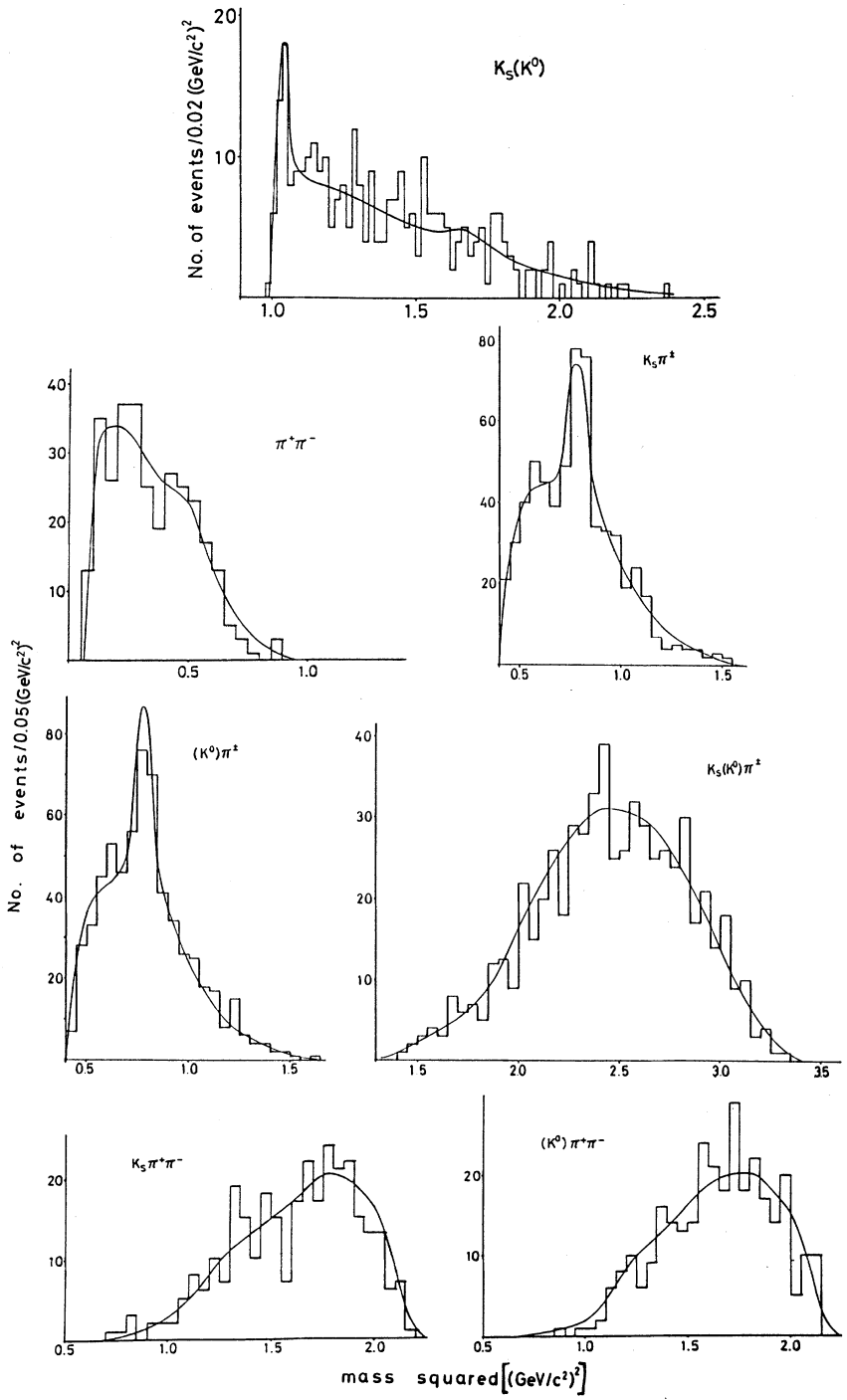

FIG. 9. The two- and three-body effective-mass-squared distributions of the $K_S^0\pi^+\pi^-(K^0)$ events. The mass combinations are indicated in the figures. See the text for the explanation of the solid curves.

TABLE IV. Resonance parameters used in fitting effective-mass-squared distributions.

	Mass^2 [(GeV/c^2)^2]	Mass×width [(GeV/c^2)^2]
$K^{*\pm}$	0.796	0.044
K^{*0}	0.803	0.044
ρ	0.602	0.12
A_2	1.72	0.13
ϕ	1.04	0.016[a]
S^*	0.96	0.039
$\delta^{\pm}(980)$	expressed by the form $1/[1+(aq)^2]$ scattering length $a=2$ fm	

[a]The width of the ϕ is enlarged to take into account the experimental resolution.

K^*, ρ, A_2, ϕ, and S^*. Except for δ, these resonances were represented by relativistic Breit-Wigner forms, and δ by the scattering-length formula used above with q being the K momentum in the $K\bar{K}$ center of mass. The parameters of the resonances used in our analysis are listed in Table IV. Fits to the experimental distributions were made by the maximum-likelihood method. The fits are shown as the solid curves in Figs. 7, 8, and 9.

The intermediate states considered for each final

TABLE V. Fractions of resonance production in the $K_S^0K^{\pm}\pi^{\mp}$, $K_S^0K^{\pm}\pi^{\mp}\pi^0$, and $K_S^0\pi^+\pi^-(K^0)$ states obtained by this experiment together with those by others.

Channel \ Momentum	1.2 GeV/c (Ref. 6)	0.73 GeV/c (Ref. 4)	All	This expt. 670−580 MeV/c	530−480 MeV/c	At rest (Ref. 1)
			Rate (%)			
$K_S^0K^{\pm}\pi^{\mp}$						
$K^{*0}K^0$	18±1	20±2	25±4	21±6	25±6	24
$K^{*\pm}K^{\mp}$	31±1	30±2	32±4	41±6	28±6	15
$A_2^{\pm}\pi^{\mp}$	6±1	13±2	12±4	13±6	5±6	14
$(K\pi)_{SL}K$	-	22±2	31±6	25±9	42±9	46
Phase space	32±7	5±2				
$K_S^0K^{\pm}\pi^{\mp}\pi^0$						
$K^{*\pm}K^{\mp}\pi^0$	13±1	11±1	13±5 (22)	21±8	20±8	
$K^{*0}K_S^0\pi^0$	8±1	7±1	13±5 (14)	14±8	17±8	
$K^{*0}K^{\pm}\pi^{\mp}$	6±1	6±1	8±5 (11)	9±7	14±7	
$K^{*\pm}K_S^0\pi^{\mp}$	7±1	10±1	16±5 (24)	24±8	19±8	
$K^{*\pm}K^{*\mp}$	14±1	17±1	9±5			
$K^{*0}K^{*0}$	5±1	6±1	3±5			
$A_2(\rho^{\mp}+\pi^{\mp}\pi^0)$	6±1	9±1	10±3 (4)	6±2	3±2	
$\delta^{\pm}\pi^{\mp}\pi^0$	2±2	8±1	11±4 (7)	12±6	2±2	
$K_S^0\pi^+\pi^-(K^0)$						
$K^*K\pi$	36±2	40±2	50±10	32±14	59±14	
K^*K^*	28±2	30±2	14±5	21±8	15±8	
$\phi\pi^+\pi^-$	5±1	3±1	12±3	10±4	13±4	
$S^*\pi^+\pi^-$	3±1	4±1	-	-	-	
$(A_2^0+f^0)(\rho+\pi\pi)$	3±1	10±1	8±2	10±3	6±3	

state and their fractions for the entire momentum region as well as for the upper and lower halves of our momentum region are listed in Table V, together with the data at rest[1,2] and at 0.73 (Refs. 3 and 4) and 1.2 GeV/c (Refs. 5 and 6).

The final state $K_S^0K^{\pm}\pi^{\mp}$ is seen to be dominated by the pseudo-two-body intermediate state K^*K. There seems to be no significant variation in the fractions of the various intermediate states from at rest to 1.2 GeV/c.

Likewise, no significant variation is observed in the fractions of the intermediates states for the final states $K_S^0K^{\pm}\pi^{\mp}\pi^0$ and $K_S^0\pi^+\pi^-(K^0)$.

A simple model based on phase space and spin multiplicities[14] predicts a value of 6 for the ratio of the phase-space-corrected production rate of a two-body state involving 0^- and 1^- mesons to that involving 0^- and 0^- mesons. It also predicts a value of 9 for the ratio $(1^-,1^-)/(0^-,0^-)$. Our values of $(K^0\bar{K}^{0*}+K^*\bar{K}_0)/K_S^0K_L^0 = 7.8\pm0.30$ and $K^{0*}K^{0*}/K_S^0K_L^0 = 8.6\pm4.4$ are not inconsistent with the predicted values.

VI. CONCLUSIONS

Many exclusive cross sections for channels with at least one K_S^0 were obtained. No clear variation with energy was observed in the cross-section behavior.

Copious resonance production was observed in three- and more-body final states. No significant variation with energy was seen in the fractions of the various resonances produced in antiproton-proton interactions from at rest to 1.2 GeV/c.

For the $K_S^0K_L^0$ final state there is a weak indication of a broad enhancement in the cross section at an incident momentum of 500 MeV/c. The angular distribution of K_S^0 seems to indicate a large D-wave contribution suggesting the formation of a $J^P=1^-$ or 3^- state in the final state.

ACKNOWLEDGMENTS

We are grateful to the operating crews of the Brookhaven AGS and 30-in. bubble chamber for their assistance during the exposure, and to the scanning and measuring crews of the University of Massachusetts and the University of Tokyo. Thanks are due also to J. Button-Shafer, R. Carson, S. Hertzbach, and R. Kofler of the University of Massachusetts who participated in the early stage of this experiment. The computation was performed at the Educational Computer Center and the Computer Center, both of the University of Tokyo, and at the Computer Centers of KEK and the LICEPP, University of Tokyo. One of us (Y.K.) wishes to express his gratitude to the Japan Society for the Promotion of Science for financial support. This work was supported in part under the auspices of the U. S. Department of Energy and the Meson Science Laboratory, University of Tokyo, and by grants from the Japanese Ministry of Education, Science, and Culture, the Toray Science Foundation, the Kurata Foundation, and the Matsunaga Foundation.

---

*Now at Wilson Laboratory, Cornell University, Ithaca, N. Y. 14853.

[1]B. Conforto *et al.*, Nucl. Phys. B3, 469 (1967).
[2]P. Baillon *et al.*, Nuovo Cimento 50A, 393 (1967).
[3]R. Nacasch *et al.*, Nucl. Phys. B135, 203 (1978).
[4]S. N. Ganguli *et al.*, Nucl. Phys. B183, 295 (1981).
[5]J. Barlow *et al.*, Nuovo Cimento 50A, 701 (1967).
[6]J. Duboc *et al.*, Nucl. Phys. B46, 429 (1972).
[7]A. Benvenuti *et al.*, Phys. Rev. Lett. 27, 283 (1971); D. Cline and R. Rutz, Phys. Rev. D 5, 778 (1972); A. Benvenuti *et al.*, Report No. CERN 72-1 027, 1972 (unpublished).
[8]R. G. Carson *et al.*, in *Proceedings of the XVIth International Conference on High Energy Physics, Chicago-Batavia, Ill., 1972,* edited by J. D. Jackson and A. Roberts (NAL, Batavia, Ill., 1973), Vol. 3, p. 61. This was a preliminary presentation of the present data.
[9]P. Petitjean, Ph.D. thesis, Universite Pierre et Marie Curie, Paris, 1977 (unpublished), cited in Ref. 4.
[10]Ch. Defoix *et al.*, in *Antinucleon-Nucleon Interactions,* proceedings of the Stockholm Symposium, 1976, edited by G. Ekspong and S. Nilsson (Pergamon, New York, 1977), p. 169.
[11]S. Sakamoto *et al.*, Nucl. Phys. B158, 410 (1979).
[12]R. R. Burns *et al.*, Phys. Rev. D 8, 1286 (1973).
[13]T. Handler *et al.*, Nucl. Phys. B110, 173 (1976).
[14]M. Kretzchmar, Ann. Rev. Nucl. Sci. 11, 1 (1961).